Mech Time-Depend Mater (2021) 25:581–600
https://doi.org/10.1007/s11043-020-09461-1

Investigation on the full Mullins effect using time-dependent hyperelastic model with energy dissipation for rubber antivibration applications

Robert Keqi Luo[1,2]

Received: 3 September 2019 / Accepted: 4 August 2020 / Published online: 1 September 2020

Abstract Despite being investigated for many years, the Mullins effect is considered a major obstacle in understanding the behavior of rubber, especially in antivibration design and applications. It is important that not all current models relate the Mullins effect with a physical rubber property and the response is not measured in real time. In this paper, we propose a new method for antivibration applications. The full Mullins effect in the modified hyperelastic model, with stress softening and residual strain from the virgin state, is assumed to be a combination of damage, energy dissipation, and time-dependent characteristics. The measurable property of rubber (i.e. rebound resilience) is included. An industrial product, a circular rubber mount used for rail vehicles, is utilized for the experiment and simulation verification. The real-time history of the load and deflection calculated from the model is compared to the experimental data. In addition, the load-deflection responses of five consecutive cycles are extracted from the simulated historical data. To verify the proposed approach further, an overloading procedure 20% beyond specification is performed on three consecutive cycles. The comparisons between the simulation and the test data, in both the time-domain and load-deflection form, demonstrate the accuracy and reliability of the proposed approach. As the hyperelastic models are widely used in industry, the modification on existing models can be easily achieved and applied to antivibration applications.

Keywords Mullins effect · Residual strain · Hyperelastic model · Time-dependent response · Energy dissipation · Cyclic stress softening

1 Introduction

Rubber components are widely used in antivibration applications. The mechanical properties of rubber materials display considerable changes during the first several loading–unloading

✉ R.K. Luo
robert.luo@trelleborg.com; Luo0801@gmail.com

1 Trelleborg Industrial Anti-Vibration Solutions, Leicester LE4 2BN, UK

2 Department of Railway Engineering, School of Civil Engineering, Central South University, Changsha, Hunan, 410075, China

cycles after molding. This observation, with both stress softening and residual strain, is known as the Mullins effect; see Mullins (1947, 1969) and Harwood et al. (1966). In engineering design, stiffness measurement is based solely on the loading portion of the loading–unloading procedure; see Luo et al. (2004) and Luo and Wu (2006). There are very limited studies on the Mullins effect on antivibration products, as profiles of rubber components are usually complex and most loading conditions involve multiaxial stress states.

Although it has been investigated for many years, the Mullins effect is still considered a major obstacle to understanding the behavior of rubber-like materials. To model the Mullins effect, a damage concept has been considered by many scientists; Ogden and Roxburgh (1999a, 1999b) used classic hyperelastic models with an additional variable to model the stress softening response; this is known as the idealized Mullins effect. Dorfmann and Ogden (2004) used two additional variables in their models to simulate the full Mullins effect, including both stress softening and residual strain. Their method has been implemented in some finite element code; see, for example, Abaqus (2018). The approach has been applied to several applications, such as Bacca et al. (2017), Chen et al. (2018), and Kumar et al. (2018). This model has been also used in a dielectric elastomer analysis (Lv et al. 2018), a bellow seal evaluation (Sasso et al. 2017) and a tyre rolling study (Sokolov et al. 2018). Praffcke and Abraham (2012) found that a simplified approach to industrial applications may be more cost effective. Consequently, models for specific applications have been developed, for example, those described by Cheng et al. (2004), Andrieux and Saanouni (1999), Gornet et al. (2012), Diani et al. (2012), and Merckel et al. (2012).

For some applications, reasonable results have been obtained by omitting some factors; see Rickaby and Scott (2012). The damage concept has also been introduced into a network model and applied to cyclic uniaxial tension stretch–stress calculations (Diani and Tallec 2019). The important fact is that not all the parameters defined in current models are related to measurable physical properties (Diani et al. 2009 and Merckel et al. 2013).

The viscoelastic approach has also been used for loading–unloading evaluations, for example, analyses of viscoelastic dampers (Xu et al. 2003, 2013, and 2016). An equivalent higher-order fractional derivative model, including the effects of temperature and frequency was developed; the model was applied to several types of viscoelastic dampers, and the numerical results were successfully verified by the experimental data (Xu et al. 2016).

In principle, the Mullins effect is related to one or more physical measurable properties of rubber materials, which should be included in the models. It has been found by Luo and Wu (2014a) and Luo et al. (2016) that the Mullins effect can be related to the rebound resilience, a key physical property (BS ISO 4662:2017 (2017) and Nagdi (1993)). Hence a function containing a single additional variable was used to simulate the stress softening behavior of rubber components. More complex methods were developed to include both stress softening and residual strain with some success (Luo et al. 2014b and Luo 2015). For now, there is neither a well-defined approach to model the Mullins effect during the design process nor suitable criteria to evaluate the effect on rubber components in engineering applications. In this paper, we propose a new approach; we assume the full Mullins effect from a virgin state to be a combination between damage, energy dissipation, and time-dependent characteristics in a modified hyperelastic model.

In this paper, we describe an experiment performed on a circular rubber mount from a virgin state. The theoretical functions and assumptions will be detailed; the finite element model and the simulation will be reported and compared with measured data; the stability of the model will be discussed; and conclusions will be presented.

2 Experiment

In rail industry, the resilient wheels of the vehicles increase the ride quality and reduce the noise generated by the interaction of the rails and wheels. One of the key design requirements for the resilient wheels is an accurate prediction of stiffness. The circular mount is made from a filled natural rubber compound with 70 hardness. It is 140 mm in diameter and 45 mm in height; it is used for resilient wheel design, as shown in Fig. 1(a).

(a) Circular wheel mount

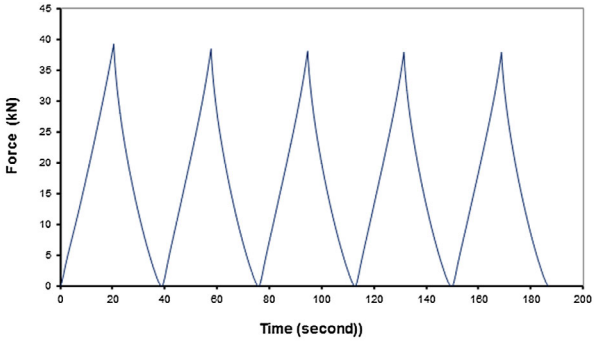

(b) Force history of the circular wheel mount

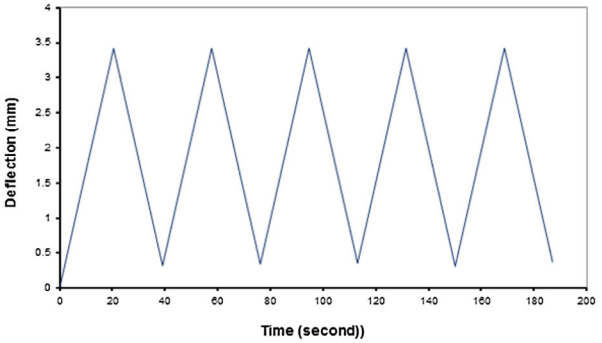

(c) Displacement history of the circular wheel mount

Fig. 1 The circular wheel mount and the experimental measurement

Fig. 1 (*Continued*)

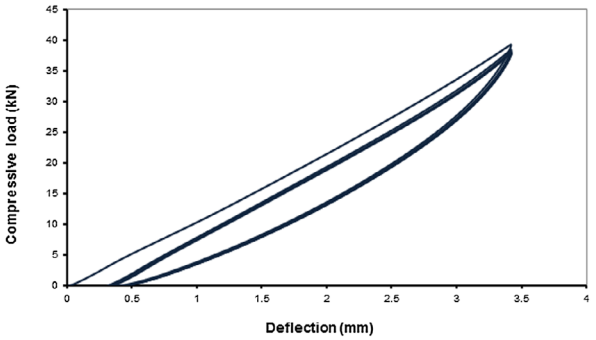

(d) Load-deflection response from a virgin state

A compressive loading procedure was performed on this circular mount from the virgin state in the laboratory, based on the specifications. In this procedure, a fixed deflection along the vertical direction was applied for five consecutive cycles up to approximately 3.5 mm at a rate of 10 mm/min. The experiment lasted approximately 190 seconds. Figure 1(b) shows the force history over the loading period, and the deflection history is displayed in Fig. 1(c). The load-deflection curve was obtained by removing the time variable, as demonstrated in Fig. 1(d). The full Mullins response was observed with both the stress softening and the residual strain. In addition to the maximum force reduction in each cycle with different loading–unloading paths, the residual deflection was also observed in an accumulated form.

3 Theoretical models

A general form of classic hyperelastic models can be written as (see Bower 2010 and Ogden 1984)

$$W = W_I(\overline{I}) + W_J(J), \tag{1}$$

where $W_I(\overline{I})$ is the deviatoric part of the strain energy density of the primary material response, and $W_J(J)$ is the volumetric part of the strain energy density. $\overline{I}$ can be further expanded to $\overline{I}_1$ and $\overline{I}_2$, which are alternative sets of the invariants of the left Cauchy–Green deformation tensor $\boldsymbol{B}$:

$$\overline{I}_1 = \frac{I_1}{J^{2/3}}, \tag{2}$$

$$\overline{I}_2 = \frac{I_2}{J^{4/3}}, \tag{3}$$

$$I_1 = \mathrm{trace}(\boldsymbol{B}), \tag{4}$$

$$I_2 = \frac{1}{2}\left(I_1^2 - \boldsymbol{B}\cdot\boldsymbol{B}\right). \tag{5}$$

The left Cauchy–Green deformation tensor $\boldsymbol{B}$ can be expressed using the deformation gradient tensor $\boldsymbol{F}$:

$$\boldsymbol{F} = \begin{Bmatrix} 1+\frac{\partial u_1}{\partial x_1} & \frac{\partial u_1}{\partial x_2} & \frac{\partial u_1}{\partial x_3} \\ \frac{\partial u_2}{\partial x_1} & 1+\frac{\partial u_2}{\partial x_2} & \frac{\partial u_2}{\partial x_3} \\ \frac{\partial u_3}{\partial x_1} & \frac{\partial u_3}{\partial x_2} & 1+\frac{\partial u_3}{\partial x_3} \end{Bmatrix} \tag{6}$$

or

$$F_{ij} = \delta_{ij} + \frac{\partial u_i}{\partial x_j}, \tag{7}$$

$$\boldsymbol{B} = \boldsymbol{F} \cdot \boldsymbol{F}^{\boldsymbol{T}}, \qquad B_{ij} = F_{ik} F_{jk}. \tag{8}$$

Let J be the Jacobian of the deformation gradient and a measure of the volume change caused by deformation:

$$J = \sqrt{\det(\boldsymbol{B})} = \det(\boldsymbol{F}) \tag{9}$$

The stress-strain law can be obtained by differentiating the strain energy density. The derivation procedure is tedious; the results are as follows:

$$\sigma_{ij} = \frac{2}{J}\left[\frac{1}{J^{\frac{2}{3}}}\left(\frac{\partial W}{\partial \overline{I}_1} + \overline{I}_1 \frac{\partial W}{\partial \overline{I}_2}\right) B_{ij} - \left(\overline{I}_1 \frac{\partial W}{\partial \overline{I}_1} + 2\overline{I}_2 \frac{\partial W}{\partial \overline{I}_2}\right) \frac{\delta_{ij}}{3} - \frac{1}{J^{\frac{4}{3}}} \frac{\partial W}{\partial \overline{I}_2} B_{ik} B_{kj}\right] + \frac{\partial W}{\partial J}\delta_{ij}, \tag{10}$$

where δ_{ij} is the Kronecker delta.

Polynomial forms of the strain energy potential are frequently used in industry:

$$W = \sum_{i+j=1}^{n} C_{ij} (\overline{I}_1 - 3)^i (\overline{I}_2 - 3)^j + \sum_{i=1}^{n} \frac{1}{D_i} (J-1)^{2i}, \tag{11}$$

where C_{ij} and D_i are material constants. The Neo–Hookean model is the simplest form of the strain energy potential

$$W = C_{10}(\overline{I}_1 - 3) + \frac{1}{D_1}(J-1)^2. \tag{12}$$

The existing models based on Eq. (1) can only be used for uploading simulation without residual strain. The models need to be modified to account for the unloading portion with residual strain. To achieve the requirement, a measurable physical property needs to be included in the modified model so that the simulation of the Mullins response can be directly linked with characteristics of rubber. The proposed model should not require a negative stress state for residual strain to be included. Finally, to match a real test procedure, the response in time-domain should be available by introducing a real-time variable.

It is postulated that the Mullins effect may be considered a combination of damage, energy dissipation, and time-dependent characteristics. The concept is that the first loading to a maximum deflection is dominated by damage, followed by energy dissipation and time-dependent response. After the first loading–unloading cycle completes, residual strain is

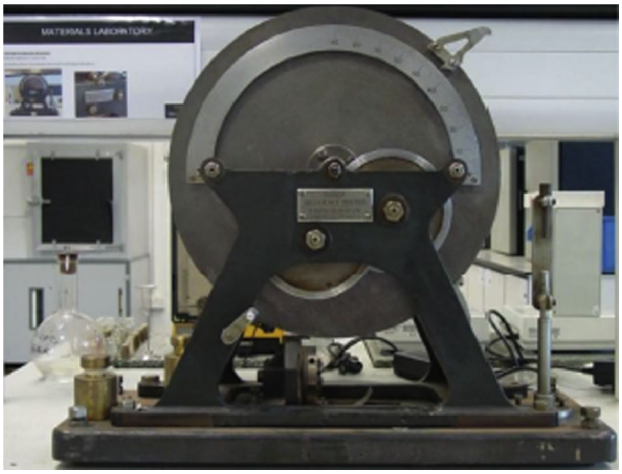

Fig. 2 Tripsometer equipment

formed and accumulates with each added reloading–unloading cycle. In addition, energy dissipation and time-dependent characteristics are added for every loading–unloading cycle. A damage index is defined as the ratio between the residual deformation and the maximum deformation:

$$D_{max} = \frac{\delta_r}{\delta_{max}}, \tag{13}$$

where δ_{max} is the deflection under the maximum load, and δ_r is the residual deflection corresponding to the maximum load. The value is expressed as a percentage.

The time-dependent response is added after the first loading:

$$R(\overline{I}, t) = k(t - T_1)^{\zeta}(\overline{I}_1 + \overline{I}_2), \tag{14}$$

where t is time, T_1 is the time when the first loading finishes, and K and ζ are parameters to be defined.

The stress softening can be related to the energy dissipation. It has been found that a physical property (i.e. the rebound resilience) can be measured to reflect the energy loss (dissipation). Hence this parameter needs to be included to calculate the softening response. The determination of the rebound resilience is standardized in BS ISO 4662:2009. A tripsometer can be used to perform the test, which is shown in Fig. 2.

To include the full Mullins effect in the classic hyperelastic model, Eq. (1) can be modified to

$$W = \theta(t) W_I(\overline{I}) + W_J(J) + R(\overline{I}, t). \tag{15}$$

During the first loading from the virgin state,

$$\theta(t) = \left(1 - \frac{t}{T_1} D_{max}\right), \quad 0 \le t \le T_1. \tag{16}$$

During the reloading,

$$\theta(t) = (1 - D_{max})\left[(1 - (1 - \theta_0)\left(1 - \frac{t - T_i}{T_{i+1} - T_i}\right)^{\eta_r}\right], \quad T_i < t \le T_{i+1}, \tag{17}$$

where θ_0 is the rebound resilience, and T_i is the time between the start and end of the loading–unloading cycle, and $i = 1, 2, 3 \ldots$, η_r is a reloading index.

During the unloading,

$$\theta(t) = (1 - D_{max})\left[(1 - (1 - \theta_0)\left(\frac{t - T_i}{T_{i+1} - T_i}\right)^{\alpha}\right]\left[1 - (1 - D_{max})\left(\frac{t - T_i}{T_{i+1} - T_i}\right)^{\eta_u}\right],$$
$$T_i < t \le T_{i+1}, \tag{18}$$

where α is the resilience index, and η_u is the unloading index.

The classic hyperelastic model (1) is modified to the time-dependent model (15), which can be used for the Mullins calculations. In model (15), because $W_I(\overline{I})$ is the function of the strain energy density, by introducing $\theta(t)$, $\theta(t)W_I(\overline{I})$ varies as the loading–unloading process develops. The rubber physical property for the energy dissipation measurement, rebound resilience, is included in $\theta(t)$. Hence the energy dissipation performance in rubber is achieved.

4 Simulation and comparisons

We generated an axisymmetric model for the circular mount due to the symmetry in both the geometry and the loading condition. The total number of degrees of freedom was approximately 4,400, in which approximately 1,400 elements were used. The type of element used was CAX4H. For clarity, a half of the solid finite element model of the circular product was displayed, as plotted in Fig. 3(a). From the rubber resilience test, the value of the rebound resilience θ_0 was 60%. The maximum damage D_{max} was approximately 9.4% at the maximum loading 39 kN. For the purpose of demonstration, the Neo–Hookean model was used for the simulation test:

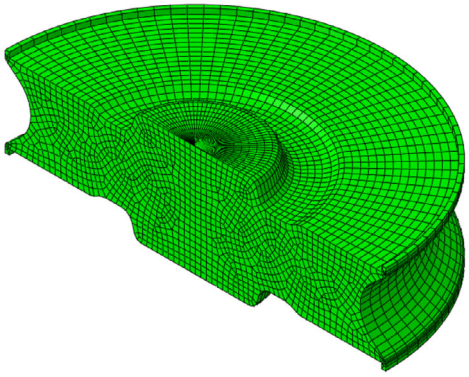

Fig. 3 Finite element model and stress profiles

(a) Finite element model for circular wheel mount

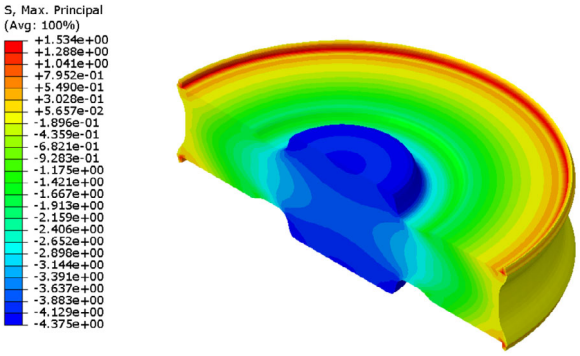

(b) The stress profile of the circular wheel mount at first maximum load

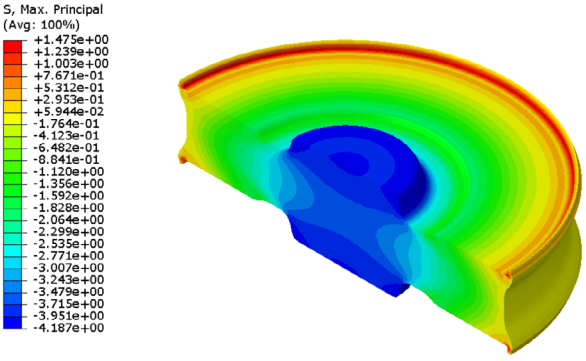

(c) The stress profile of the circular wheel mount at second maximum load

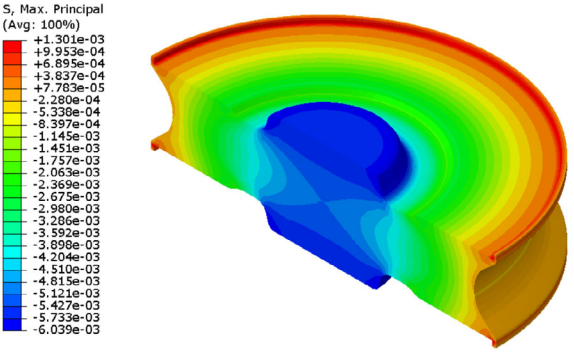

(d) The stress profile of the circular wheel mount at the end of first unloading

Fig. 3 (*Continued*)

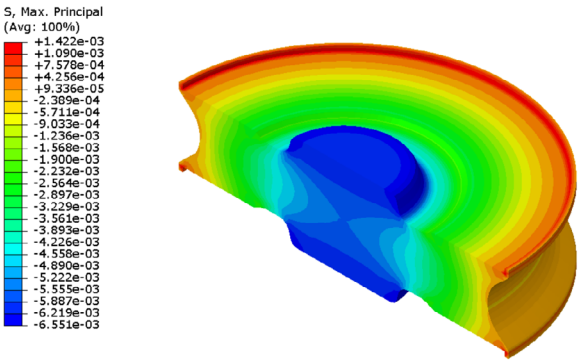

(e) The stress profile of the circular wheel mount at the end of second unloading

Fig. 3 (*Continued*)

$$C_{10} = 0.92; \qquad D_1 = 0.00165.$$

The entire experimental procedure was simulated, and the values of the parameters to be defined for the Mullins simulation were:

$$k = -0.012,$$
$$\zeta = 0.1,$$
$$\alpha = 0.5,$$
$$\eta_r = \eta_u = 5.0.$$

The parameters C_{10} and D_1 were extracted from standard material tests (uniaxial, biaxial, planer, and volumetric tests) and verified by actual products, and α is a constant (an optimized value for the idealized Mullins prediction from Luo (2020)). The remaining parameters were determined by the data-fitting procedure.

The maximum stress profiles between the first maximum loading from the virgin state and the second maximum loading are demonstrated in Figs. 3(b) and 3(c). Although the values were different, the pattern of the two stress contours were similar. The stress value from the first loading was approximately 1.53 MPa against approximately 1.41 MPa from the second loading, with approximately 4% difference. Due to the damage and some contributions from the time-dependent response, there were residual deformations in the mount when the loading forces were removed, as shown in Fig. 1(d). Figure 3(d) and 3(e) reveal the maximum stress values of 0.0013 MPa and 0.0014 MPa at the end of the first and second unloadings, respectively, which corresponds to zero load. It should be pointed out that this model did not require a negative stress state to contain the residual strain. Figure 4(a) illustrates the simulated load-deflection curve for five consecutive loading–unloading cycles, which was nearly identical to the measurement shown in Fig. 1(d). Figure 4(b) and (c) show the comparison of force and deflection history between the experiment and simulation, respectively. The comparison demonstrates the accuracy of the proposed model. Finally, a detailed com-

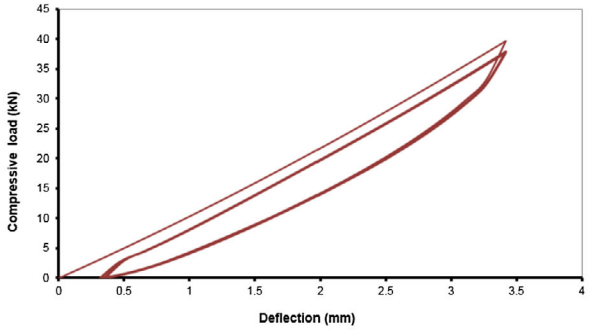

(a) Simulation on experimental loading-unloading cycles

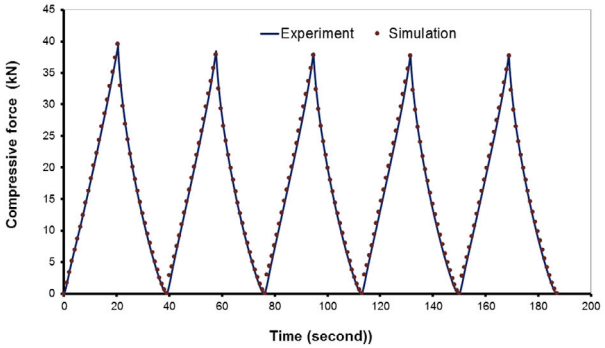

(b) Comparison of Force history between the experiment and the simulation

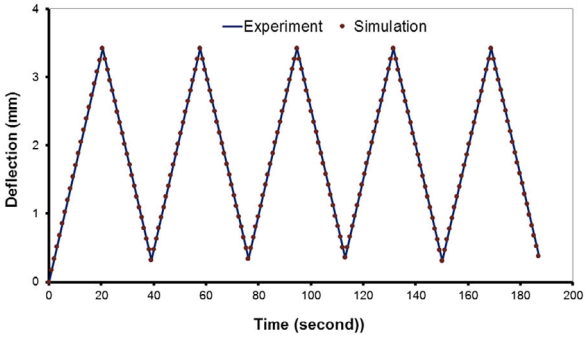

(c) Comparison of deflection history between the experiment and the simulation

Fig. 4 Simulation result and comparison with experimental results

parison on load-deflection between the experiment and simulation for all individual cycles, ranging from cycle 1 to cycle 5, are presented in Fig. 5. The comparison indicates that the model well evaluated the Mullins effect for rubber antivibration applications.

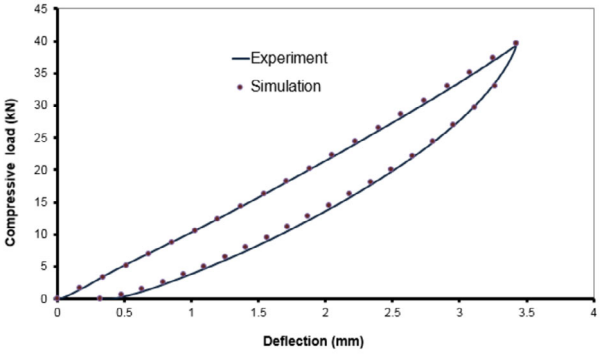

(a) The 1st load-deflection comparison between the experiment and the simulation

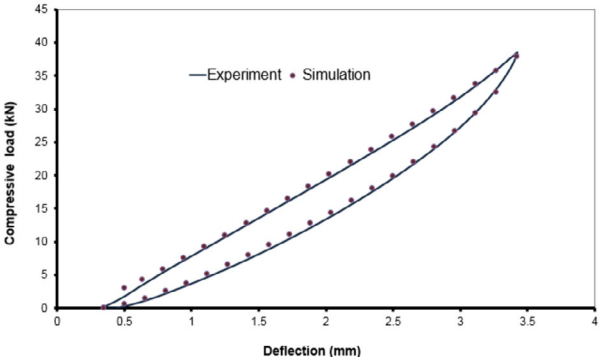

(b) The 2nd load-deflection comparison between the experiment and the simulation

Fig. 5 Load-deflection comparison between the experiment and the simulation

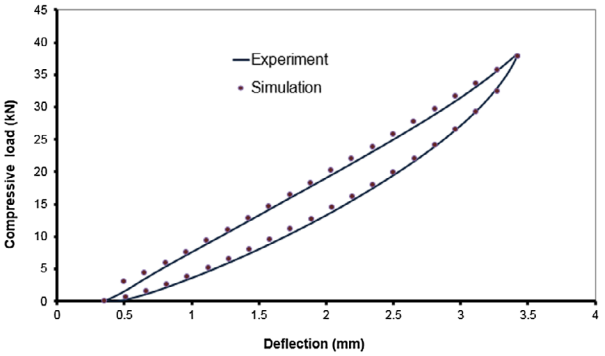

(c) The 3rd load-deflection comparison between the experiment and the simulation

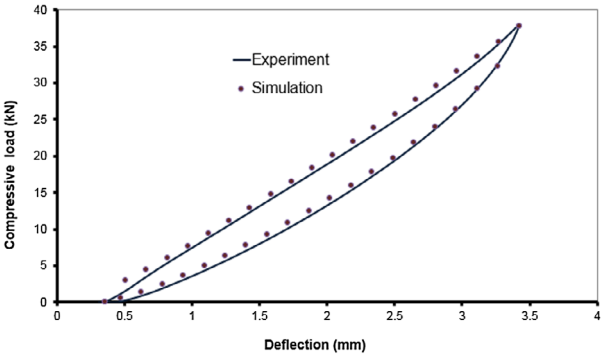

(d) The 4th load-deflection comparison between the experiment and the simulation

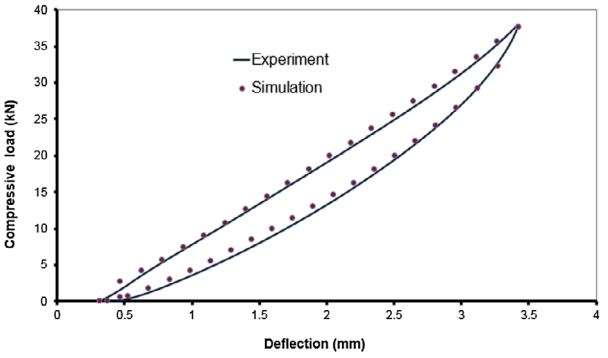

(e) The 5th load-deflection comparison between the experiment and the simulation

Fig. 5 (*Continued*)

5 Discussion

In industry a typical tolerance of stiffness specification of an antivibration product is ±20%. Using this criterion, we carried out an investigation of different parameters to examine the stability and accuracy of the proposed approach.

5.1 Time-dependent function $R(\overline{I}, t)$

This equation is a continuous creep function with two parameters k and ζ; k can be considered an amplitude parameter that determines the strength of the creep, and ζ may be taken as a hardening coefficient that governs how quickly the creep progresses within the time frame.

The time-dependent function is not active until the first loading finishes as the damage is dominated over this initial loading from the virgin state. For clarity, the first two complete cycles are displayed in Fig. 6. It shows that the change of the amplitude parameter k had slightly bigger influence on the response than that of the hardening coefficient ζ. However,

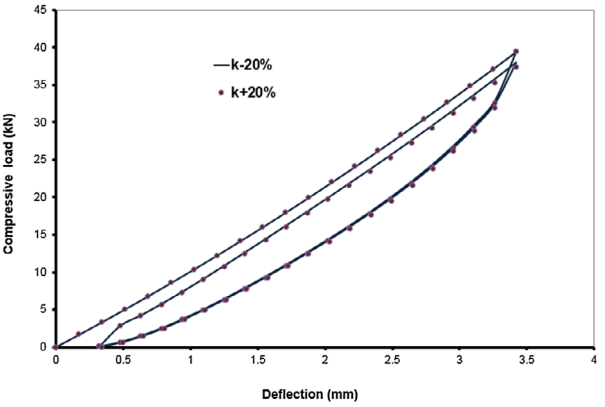

(a) The effect from parameter k

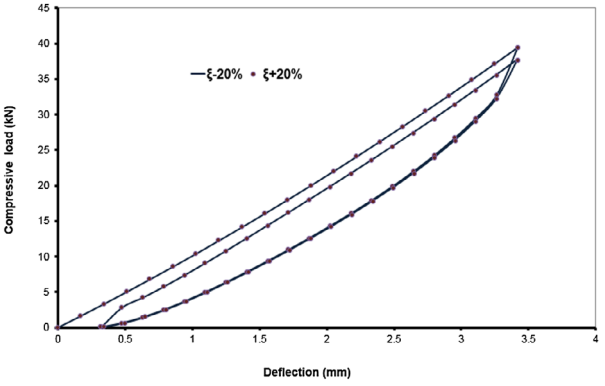

(b) The effect from parameter ξ

Fig. 6 The effect from the time dependent function

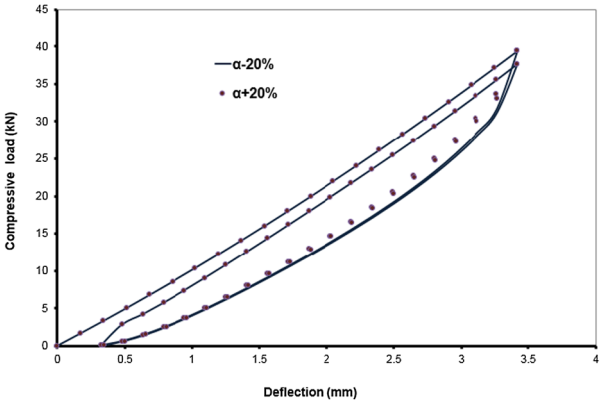

Fig. 7 The effect from the rate of energy dissipation

all the influences were small due to this relatively short period of measurement. After a much longer time period, the effect is more apparent. A typical example is a creep simulation on a rubber product up to 2000 hours using a similar function conducted by Luo (2019).

5.2 The resilience index α

The resilience index α characterizes the strain energy stored in the rubber; its reciprocal is the rate of energy dissipation. The lower the resilience index, the higher its reciprocal, and the faster the strain energy releases when an unloading begins. The index α is active only during unloading. Figure 7 illustrates the effect of changing α. There are some effects on the response at the beginning of the unloading. The largest difference should be seen when the loading ends and the unloading begins. Since the value of α has properly been tested (Luo 2020), the effect of the deviation is limited.

5.3 The reloading index η_r and the unloading index η_u

The effects from both indices were almost the same, and nearly no apparent effect was observed on the response, as illustrated in Fig. 8. The reason for this is that both indices play a similar role in $\theta(t)$, and these parameters have been selected properly. Therefore it may be much simpler to assign the same value to both variables, which is the case in this application.

By the previous results the proposed approach was stable, and the simulated response was not highly sensitive to a reasonable change of the parameters. The deviation range $\pm 20\%$ of the parameters, based on a typical industrial specification, had limited influences on the Mullins response, which implies that a reasonable range of values were available for those coefficients. Therefore it should not be difficult to find suitable values to evaluate the Mullins effect in antivibration applications.

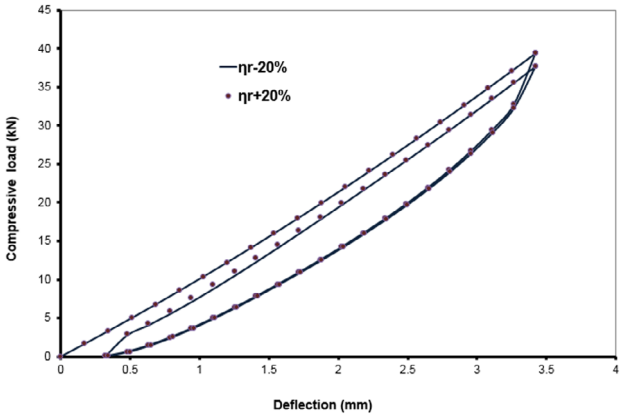

(a) The effect from the reloading index

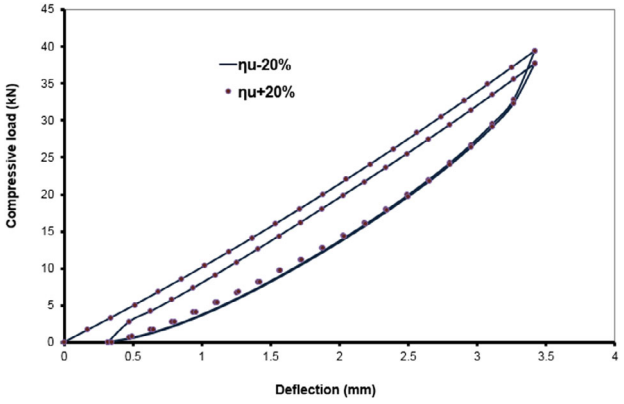

(b) The effect from the unloading index

Fig. 8 The effect from the reloading and the unloading index

5.4 Overloading case

To test the approach further, approximately 20% overloading was applied to the rubber component with the same compound in three consecutive loading–unloading cycles. All the parameters remained the same except for the maximum damage, which was approximately 6.1% at the maximum load of 48 kN. Figure 9(a) shows the maximum stress profile under the first maximum loading, which was approximately 30% higher than that in the normal loading. As shown in Fig. 9(b), the maximum stress profile at the end of the first unloading was approximately 0.0004 MPa, which corresponded to the zero load. The load-deflection curves of the three consecutive cycles, which are plotted in Figs. 10(a) and 10(b), demonstrate excellent agreement with the experimental data, as illustrated in Figs. 10(c), (d), and (e). From the prediction perspective, not based solely on the simulation, reasonable agreement was seen between the predicted results and the measured response when all the parameters from the normal loading were used.

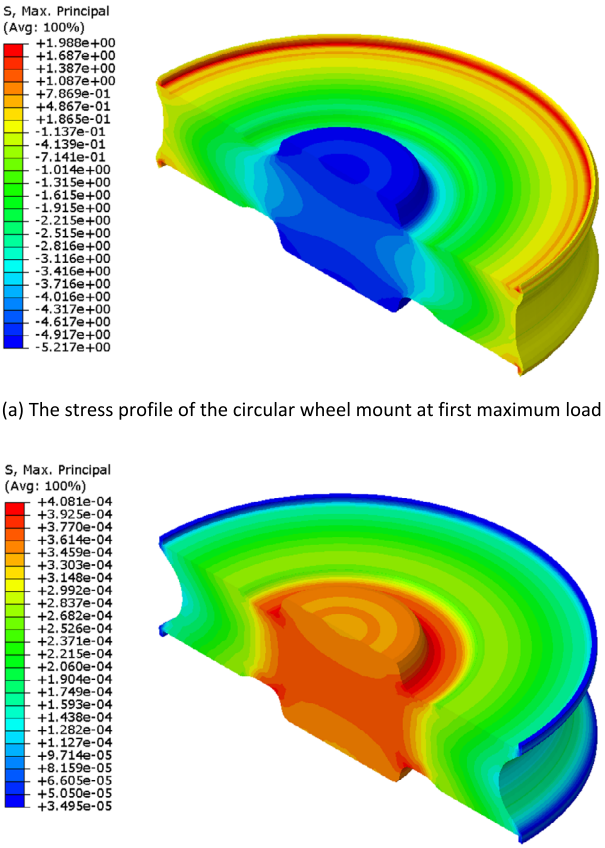

Fig. 9 Stress profiles between the end of the first loading and the first unloading for overloading condition

(a) The stress profile of the circular wheel mount at first maximum load

(b) The stress profile of the circular wheel mount at the end of first unloading

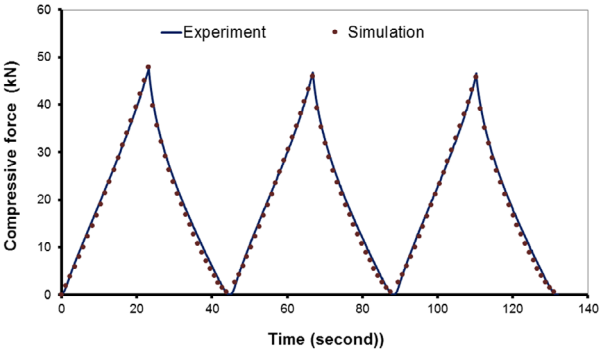

(a) Comparison of Force history between the experiment and the simulation

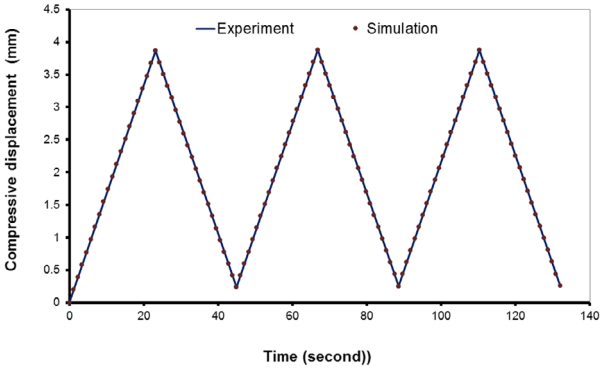

(b) Comparison of deflection history between the experiment and the simulation

Fig. 10 Comparison between the simulation and the experiment for overloading condition

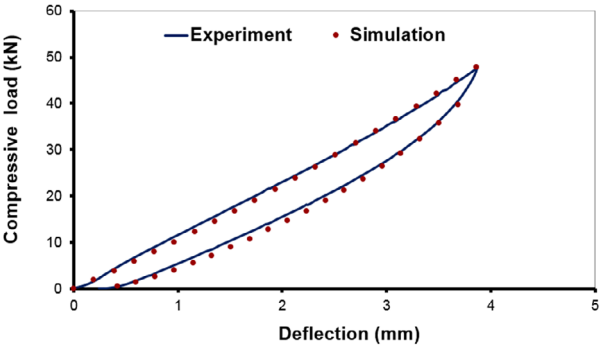

(c) The 1st load-deflection comparison between the experiment and the simulation

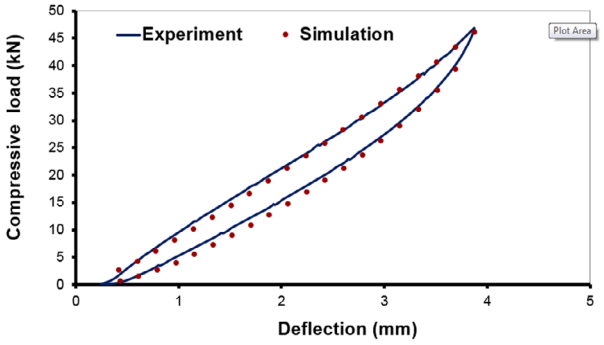

(d) The 2nd load-deflection comparison between the experiment and the simulation

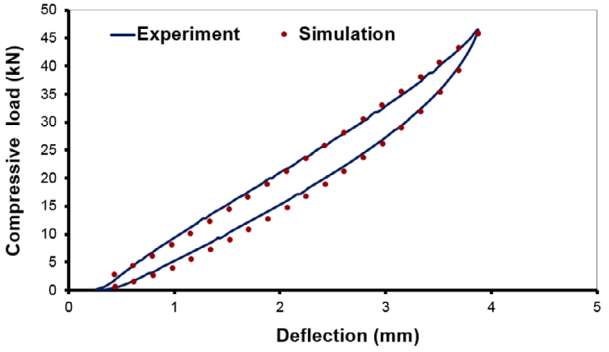

(e) The 3rd load-deflection comparison between the experiment and the simulation

Fig. 10 (*Continued*)

6 Conclusion

In this study, we proposed a new model to simulate the full Mullins effect for an antivibration component. The damage concept, energy dissipation, and time dependent behavior are all included in the model, which can be used to obtain the Mullins response from the virgin state. This model incorporates a physically measurable property of rubber materials (i.e. the rebound resilience). To verify this approach, a circular mount for a resilience wheel used in rail vehicles was tested based on the specification. The real-time history for load-deflection response was calculated and compared with the experimental data. In addition, the load-deflection response of five consecutive cycles were extracted from the historical data. The comparisons between the simulation and the test data, in both the time-domain and load-deflection form, have demonstrated the accuracy and reliability of the proposed approach. For further verification, an overloading procedure above the specification has been carried out on three consecutive cycles. The results of this procedure have also demonstrated the accuracy of the proposed method. Particular attention should be paid to the fact that the proposed model does not require a negative stress state to include the residual strain. Hyperelastic models are widely used in industry, and the modification of existing models can be achieved easily and effectively. Nevertheless, the proposed approach should be further verified using more engineering cases.

Acknowledgements The author would like to thank Mr. John Simmonds, Mr. Jonathan Foster, and Mr. David Moore at Trelleborg AVS (U.K.) for their technical support. Theoretical discussions with colleagues in Central Southern University are also appreciated. The comments, suggested by the reviewer, have greatly enhanced the investigation.

Declaration of conflicting interests The author declares that there is no conflict of interest.

References

Andrieux, F., Saanouni, K.: On a damaged hyperelastic medium: Mullins effect with irreversible strain. Int. J. Damage Mech. **8**(1), 82–101 (1999)

Bacca, M., Creton, C., McMeeking, R.: A model for the Mullins effect in multinetwork elastomers. J. Appl. Mech. **84**, 121009 (2017)

Bower, A.: Applied Mechanics of Solids. CRC Press, USA (2010)

BS ISO 4662:2017: Rubber, Vulcanized or Thermoplastic – Determination of Rebound Resilience. BSI British Standards Limited, London (2017)

Chen, Y., Kang, G., Yuan, J., et al.: Uniaxial ratchetting of filled rubber: experiments and damage-coupled hyper-viscoelastic-plastic constitutive model. J. Appl. Mech. **85**, 061013 (2018)

Cheng, M., Chen, W., Song, B.: Phenomenological modelling of the stress-stretch behaviour of EPDM rubber with loading –rate and damage effects. Int. J. Damage Mech. **13**, 371–381 (2004)

Dassault Systems: Abaqus User Manual. Dassault Systems, USA (2018)

Diani, J., Tallec, L.P.: A fully equilibrated microsphere model with damage for rubber like materials. J. Mech. Phys. Solids **124**, 702–713 (2019)

Diani, J., Fayolle, B., Gilormini, P.: A review on the Mullins effect. Eur. Polym. J. **45**(3), 601–612 (2009)

Diani, J., Merckel, Y., Brieu, M.: Modelling Mullins and cyclic stress-softening in filled Rubbers. In: Jerrams, S., Murphy, N. (eds.) Constitutive Models for Rubber VII, pp. 229–234. Taylor & Francis, London (2012)

Dorfmann, A., Ogden, R.W.: A constitutive model for the Mullins effect with permanent set in particle-reinforced rubber. Int. J. Solids Struct. **41**, 1855–1878 (2004)

Gornet, L., Marckmann, G., Desmorat, R., et al.: A new isotropic hyperelastic strain energy function in terms of invariants and its derivation into a pseudo-elastic model for Mullins effect: application to finite element analysis. In: Jerrams, S., Murphy, N. (eds.) Constitutive Models for Rubber VII, pp. 265–271. Taylor & Francis, London (2012)
Harwood, J.A.C., Mullins, L., Payne, A.R.: Stress softening in natural rubber vulcanizates. Part II. Stress softening effects in pure gum and filler loaded rubbers. Rubber Chem. Technol. **39**, 814–822 (1966)
Kumar, N., Patel, B.P., Rao, V.V., et al.: Compressibility, damage and age hardening effects of solid propellants using finite strain constitutive model. J. Eng. Mater. Technol. (2018). https://doi.org/10.1115/1.4042661
Luo, R.K.: Mullins damage effect on rubber products with residual strain. Int. J. Damage Mech. **24**(2), 153–167 (2015)
Luo, R.K.: Creep prediction with temperature effect and experimental verification of rubber suspension components used in rail vehicles. J. Mech. Eng. Sci. **233**(11), 3950–3963 (2019)
Luo, R.K.: Complete loading-unloading-deflection prediction for antivibration system design using an energy dissipation approach. Proc. IMechE Part L, J. Mater., Des. Appl. **234**(6), 859–872 (2020)
Luo, R.K., Wu, W.X.: Fatigue failure analysis of anti-vibration rubber spring. Eng. Fail. Anal. **13**(1), 110–116 (2006)
Luo, R.K., Wu, X.P.: Simulation and experiment on rubber components using rebound energy approach with stress softening. J. Strain Anal. Eng. Des. **49**(2), 76–85 (2014a)
Luo, R.K., Wu, W.X., Cook, P.W., Mortel, W.J.: An approach to evaluate the service life of rubber springs used in rail vehicle suspensions. J. Rail Rapid Transit **218**(2), 173–177 (2004)
Luo, R.K., Peng, L.M., Wu, X.P.: Mullins effect modelling and experiment for anti-vibration systems. Polym. Test. **40**, 304–312 (2014b)
Luo, R.K., Mortel, W.J., Wu, X.P.: Evaluation of stress softening on rubber suspension used in rail vehicles. J. Rail Rapid Transit **230**(1), 15–23 (2016)
Lv, X., Liu, L., Liu, Y., et al.: Electromechanical modeling of softening behavior for dielectric elastomers. J. Appl. Mech. **85**, 111010 (2018)
Merckel, Y., Brieu, M., Diani, J., Berghezan, D.: Effect of material and mechanical parameters on the stress-softening of carbon-black filled rubbers submitted to cyclic loadings. In: Jerrams, S., Murphy, N. (eds.) Constitutive Models for Rubber VII, pp. 253–257. Taylor & Francis, London (2012)
Merckel, Y., Brieu, M., Diani, J., et al.: Understanding and modelling the Mullins softening from a mechanical point of view. In: Gil-Negrete, Alonso (eds.) Constitutive Models for Rubber VIII, pp. 411–417. Taylor & Francis, The Netherland (2013)
Mullins, L.: Effect of stretching on the properties of rubber. J. Rubber Res. **16**, 275–289 (1947)
Mullins, L.: Softening of rubber by deformation. Rubber Chem. Technol. **42**, 339–362 (1969)
Nagdi, K.: Rubber as an Engineering Material: Guideline for Users. Hanser Publishers, Germany (1993)
Ogden, R.W.: Non-linear Elastic Deformations. Ellis Horwood, Chichester (1984)
Ogden, R.W., Roxburgh, D.G.: A pseudo-elastic model for the Mullins effect in filled rubber. Proc. R. Soc. Lond. A **455**, 2861–2878 (1999a)
Ogden, R.W., Roxburgh, D.G.: An energy-based model of the Mullins effect. In: Dorfmann, A., Muhr, A. (eds.) Constitutive Models for Rubber, pp. 23–28. Balkema, Rotterdam (1999b)
Praffcke, J., Abraham, F.: Potentials of FEA-simulation for elastomer stress softening in engineering practice. In: Jerrams, S., Murphy, N. (eds.) Constitutive Models for Rubber VII, pp. 375–380. Taylor & Francis, London (2012)
Rickaby, S., Scott, N.: The Mullins effect. In: Jerrams, S., Murphy, N. (eds.) Constitutive Models for Rubber VII, pp. 273–276. Taylor & Francis, London (2012)
Sasso, M., Chiappini, G., Rossi, M., et al.: Structural analysis of an elastomeric bellow seal in unsteady conditions: simulations and experiments. Int. J. Mech. Mater. **13**, 347–362 (2017)
Sokolov, A.K., Svistkov, A.L., Shadrin, V.V., et al.: Influence of the Mullins effect on the stress–strain state of design at the example of calculation of deformation field in tyre. Int. J. Non-Linear Mech. **104**, 67–74 (2018)
Xu, Z.D., Shen, Y.P., Zhao, H.T.: A synthetic optimization analysis method on structures with viscoelastic dampers. Soil Dyn. Earthq. Eng. **23**(8), 683–689 (2003)
Xu, Z.D., Xu, C., Hu, J.: Equivalent fractional Kelvin model and experimental study on viscoelastic damper. J. Vib. Control **21**(13), 2536–2552 (2013)
Xu, Z.D., ASCE, A.M., Liao, Y.X., et al.: Experimental and theoretical study of viscoelastic dampers with different matrix rubbers. J. Eng. Mech. **142**(8), 04016051 (2016)